Optimal periodic control of power harvesting tethered airplanes: how to fly fast without wind and without propellor?

Joris Gillis, Jan Goos, Kurt Geebelen, Jan Swevers and Moritz Diehl

***Abstract*— This paper proposes *reversed pumping* as a strategy to keep tethered kites airborne in a wind-free condition without any on-board propulsion. In the context of *kite power*, it is shown to be a necessary addition to a *rotational start-up* scheme [1]. The enhanced scheme ultimately allows for injection into power harvesting orbits at high altitude, in case no wind is present near ground level. The need for reversed pumping is advocated with scaling laws, and is demonstrated in simulation by solving a proposed open-loop periodic optimal control problem. The obtained periodic orbits can be used as reference for feedback control.**

I. Introduction

For many years, mankind has been exploiting wind energy. Sailing ships and windmills have been used for many centuries. It was not until 1887 when Prof. James Blyth of the Anderson's College built the first windmill to generate electric power. Although today's wind turbines are more efficient than those from the 19$^{\text{th}}$ and the beginning of the 20$^{\text{th}}$ century, they still require a large construction to harvest comparatively little power. On the other hand, the outer part of the blades of a wind turbine is quite efficient in terms of power extraction per square meter of wing area. The inner part of the blades, the tower and the foundation serve mostly to support this outer part.

A new technology, first proposed by Loyd in 1980 [2] and often referred to as *crosswind kite power*, uses tethered airplanes[1] to harvest wind energy. There are two main possibilities on how to produce electricity with such a system. In the first mode, *lift mode*, the lift force vector does work. This is commonly implemented as a *pumping cycle*. The airplane delivers a high tension on the tether which is anchored to a ground-based generator. By unrolling the tether, the generator produces electricity. Once the tether is fully unrolled, the airplane is steered such that the force on the tether is reduced, and the tether is wound back, thus performing a pumping motion.

The second mode of generation is *drag mode*, which implies the generator being on board the airplane. This generator is driven by inversed propellers. The generated electricity is transmitted to the ground via the tether, whose length is now fixed. A system using this mode is also known as an *airborne wind turbine*.

Advantages of kite power with respect to wind turbines are that less material is needed – see Figure 1a – to harvest wind energy from a higher altitude. As altitude increases, the wind becomes stronger and more consistent. Since the power in the wind is proportional to the cube of the wind speed, there is a huge incentive to harvest wind energy from greater altitudes. At the downside there is the necessity of a robust control system and the safety issues regarding such a system operating in the vicinity of people.

Various research groups and companies in the R&D phase investigating *kite power* have emerged[3], [4], [5]. Unpublished achievements in this young field include hour-long autonomous flight with multi-kilowatt systems by companies Makani Power and KiteGen [4].

While others have investigated optimization of power harvesting orbits[6], [7], this paper deals with the question of how to reach such orbits. In particular, it builds on the idea[1] of *rotational start-up* which is useful for systems working in *lift mode* and introduces *reversed pumping* to complement it. This paper is organized as follows. Section II explains *rotational start-up* for the problem of starting and landing and describes the hardware setup that implements this idea. Section III describes a mathematical model of the set-up. Section IV describes the limitations of the proposed start-up scheme and introduces *reversed pumping* as a solution to these limitations. Finally, Section V presents numerical results for *reversed pumping* obtained by use of optimal control methods, with the help of the recently developed `ACADO Toolkit` [8].

II. Test platform for rotational start-up

This section explains the concept of *rotational start-up* and describes the hardware setup that implements it. This setup's constraints are used for all optimization and simulation results in this paper.

A. Starting and landing

One way to start and land a kite power system is using the *rotational start-up* [1]. This means that before starting, the airplane is fixed to a rotating platform, a *carousel*. Figure 1b shows a setup where the airplane wings are vertical. The carousel starts turning, bringing the airplane up to speed.

All authors are with the Katholieke Universiteit Leuven, Belgium

J. Gillis, K. Geebelen and J. Swevers are with the Department of Mechanical Engineering, K.U. Leuven, Celestijnenlaan 300B, 3001 Leuven, Belgium {`joris.gillis, kurt.geebelen, jan.swevers`}`@mech.kuleuven.be`

J. Goos is a master student with the Department of Computer Science, K.U. Leuven, Celestijnenlaan 200a, 3001 Heverlee, Belgium `jan.goos@student.kuleuven.be`

M. Diehl is with the Department of Electrical Engineering, K.U. Leuven, Celestijnenlaan 300B, 3001 Leuven, Belgium `moritz.diehl@esat.kuleuven.be`

M. Diehl is the corresponding author.

J. Gillis is a fellow of the Research Foundation – Flanders (FWO)

[1]The technology is applicable to rigid (airplane) or flexible (kite) wings.

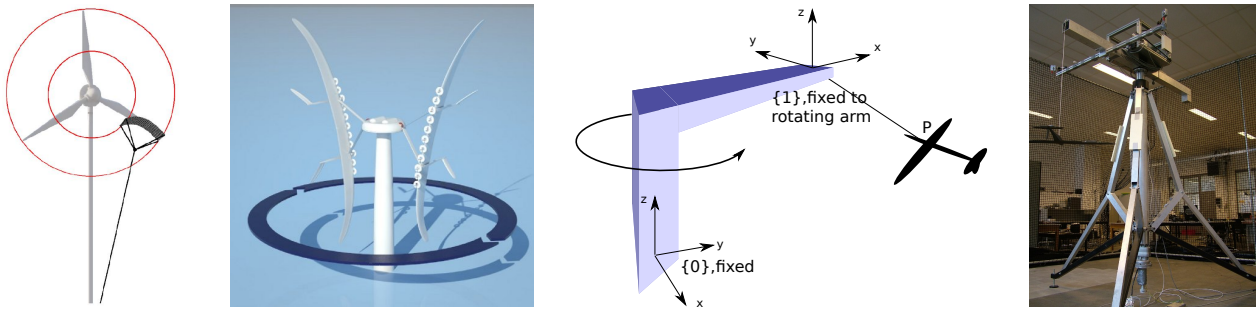

(a) (b) (c) (d)

Fig. 1. Kite power in theory and practice. (a) Kite power portrayed as outperforming classical wind turbines in material efficiency. Courtesy of B. Houska. (b) Artist's rendition of a rotational start-up implementation. Courtesy of R. Paelinck. (c) Sketch of rotational start-up: an arm tows the airplane around (c) Photograph of the test platform at K.U.Leuven. The airplane, anchored at a point close to the center of mass, can be seen hanging at the left.

The tether is unrolled while the airplane rolls so that wings become horizontal. Once past the stall speed[2], the airplane can start to gain altitude. Finally the airplane is injected into a power harvesting orbit downwind i.e. the typical figure-eight. In this paper, we do not consider competing schemes of starting and landing such as vertical take-off [5] and crane suspension [9].

B. Available hardware

A test platform capable of performing the rotation start for model airplanes is being developed at the K.U. Leuven [10], see Illustration 1d. The small dimensions of the test setup allow experiments to be done indoors, without external disturbances from wind or rain. The base of this test setup is the carousel, which is 2.5 m high, has a turning radius of 1 m and a rotation speed up to 90 rpm. The airplane has a wingspan of 1 m, with the possibility of scaling up to 2 m wingspan. The aim of this setup is to demonstrate novel control strategies for kite power, not to demonstrate actual power production.

III. Model

A simplified mathematical model of the airplane+carousel system, based on previous work by Diehl [11] & Houska [12], was developed in [10] and is used for the numerical simulations presented in Section V.

A. Assumptions

The system under investigation contains only the tether and the airplane. The tether is assumed to be perfectly straight. It is treated as a rigid bar with varying length, with a constraint such that compression forces are prohibited. Neglect of tether bending is safe for the small tether lengths investigated in this paper. The inertias are reduced to a single rigid body at the end of the cable, where distributed load on the system is concentrated as equivalent forces and torques. Conventional aerodynamics is used, which presumes the wings to experience a uniform steady state flow.

[2]The stall speed is the speed below which the airplane cannot create enough lift to sustain its own weight in flight.

B. Dynamics

The forces and torques considered are due to 1) aerodynamics of the airplane, using the small-angle approximations of conventional aerodynamics 2) drag on the cable, treated as the integrated effect of perpendicular flow impinging on a cylinder, where the local flow used stems from perpendicularly projecting the effective wind on the tether 3) force of the cable and its torque due to the anchor point not coinciding exactly with the center of mass 4) ad-hoc added damping, proportional to roll/pitch/yaw rates 5) gravity.

C. Kinematics

The model contains 7 generalized coordinates: 3 spherical coordinates (azimuth ϕ, elevation θ, radius r) to describe the position of the body's center of mass with respect to the carousel arm, a set of roll pitch yaw angles (R, P, Y), and an angle δ to describe the position of the carousel's arm. Angle of attack α and side slip angle β, explained in Figure 2a, can be expressed as an explicit function of these coordinates, their rates of change and the external wind w. For more details on the model, we refer to [10].

D. Parameters

Model parameters have been estimated or measured roughly to match the experimental setup. The most important parameter and their estimated values can be found in Table I. For a full list, we refer to [10].

Symbol	Description [unit]	Value
A	wing surface area [m^2]	0.10
C_L	maximum lift coefficient [-]	1.00
C_D	drag coefficient at maximum C_L [-]	0.06
ρ	air density [kg/m^3]	1.23
m	airplane mass [kg]	0.50
d_c	tether diameter [mm]	3.00

TABLE I

Important parameters of the model

E. States & controls of the full model

With the tether seen as a constraint on a rigid body, the airborne system has 5 degrees of freedom. This results in

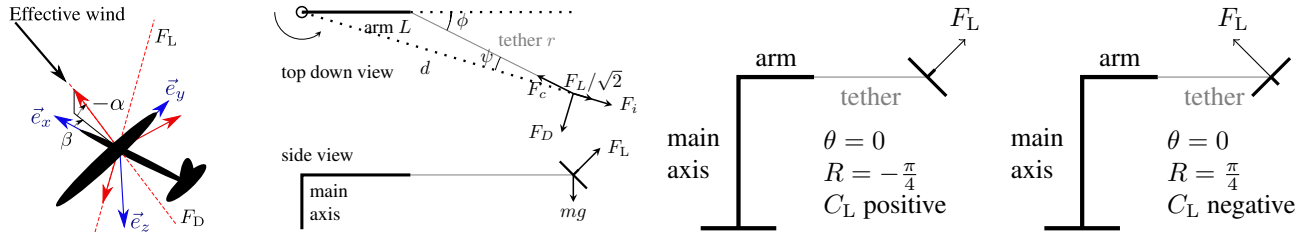

(a) (b) (c) pulling phase (d) relaxing phase

Fig. 2. Sketches for scaling analysis. (a) Airplane aerodynamics. Lines of action of lift F_L and drag F_D are indicated. (b) Steady state circular towing for $\theta = 0$ and $R = -\frac{\pi}{4}$. (c) Basic scheme for reversed pumping.

10 core system states. The airplane is controlled with an elevator ν and an aileron μ. Tether length r is the last control input. The model is expanded with extra states to increase the order of the continuity of controls and to be able to formulate constraints on rates of change of the control inputs. Additional states are added to integrate power consumed by the carousel $\dot{E}_c$ and the winch $\dot{E}_w$ over time. A state Ξ_p is used to integrate potential energy E_p over time. Consult Table II for an overview.

F. States & controls of the point model

In the point model, the dimension is further reduced by neglecting the rotational dynamics of the airplane. The airplane is assumed to instantaneously align itself with the effective wind vector. This simplification is motivated by the observation that the pitch-alignment and yaw-alignment have small natural time constants and are significantly dampened. Pitch and yaw angles P and Y become explicit functions of the effective wind vector, while α and β are taken identically zero. The remaining rotational degree of freedom R is treated as a control input. The lift-coefficient C_L, which in the full model is a dependent quantity linear in α, is treated as a control input. Consult Table II for an overview. We introduce the notation $\underline{u}$ to group all controls and $\underline{q}$ to group all states.

The point model describes well the situation in which the airplane has high bandwidth inner control loops that a) control angle of attack – and hence lift – using elevator actuation and b) control roll using aileron actuation.

The downside of the point model with respect to the full model is the obvious neglect of system instability in the rotational degrees of freedom. However, we do not propose to use the orbits resulting from this simple model in an open-loop setting – although one group[13] demonstrates it on their hardware – but rather to use them as tracking reference for a model predictive controller.

Full model		Point model
$\ddot{\delta}$, $\dddot{r}$, $\dot{\mu}$, $\dot{\nu}$	Control inputs	$\ddot{\delta}$, $\dddot{r}$, $\dot{R}$, $\dot{C}_L$
δ, $\dot{\delta}$, r, $\dot{r}$, μ, ν	Control states	δ, $\dot{\delta}$, r, $\dot{r}$, R, C_L
ϕ, θ, R, P, Y	Core states	ϕ, θ
$\dot{\phi}$, $\dot{\theta}$, $\dot{R}$, $\dot{P}$, $\dot{Y}$		$\dot{\phi}$, $\dot{\theta}$
E_c, E_w, Ξ_p	Additional states	E_c, E_w, Ξ_p

TABLE II

MODEL STATES & CONTROLS

G. Constraints

The model is only valid under the constraints enlisted in Table III.

Bounds		[unit]	Description
-0.2 $\leq \alpha,\beta$	≤ 0.2	[rad]	Small angle approx. for aerodynamics
-1 $\leq C_L$	≤ 1	[-]	Avoid stall condition of wing
4 $\leq F_c$	≤ 50	[N]	Cable must be under tension. Winch determines maximum force.
-1.5 $\leq$ R	≤ 1.5	[rad]	Avoid wing touching the tether
-10 $\leq \dot{\delta}$	≤ 10	[rad/s]	Maximum carousel speed
-5 $\leq \dot{r}$	≤ 5	[m/s]	Maximum tether speed due to winch
-10 $\leq \ddot{r}$	≤ 10	[m/s^2]	Maximum acceleration of winch
	$\dot{E}_w \leq 250$	[W]	Maximum winch power
-6 $\leq \dot{R}$	≤ 6	[rad/s]	Maximum roll rate
-8 $\leq \dot{C}_L$	≤ 8	[-]	Maximum lift change rate

TABLE III

OVERVIEW OF CONSTRAINTS UNDER WHICH MODEL ASSUMPTIONS ARE VALID AND CONSTRAINTS THAT ARE COMPATIBLE WITH THE LIMITS OF THE TEST-SETUP

IV. PHYSICAL LIMITATIONS OF ROTATIONAL START-UP

This section discusses steady-state behavior of the system when in a situation of no external wind. It is found that at a certain tether length, the airplane cannot further be driven by the towing action of the rotating arm, and will have to be driven by *reversed pumping* if not enough wind is present to provide power. This involves periodically unrolling and retracting the tether in a net energy consuming cycle.

A. Circular towing scale analysis

During *circular towing* the carousel revolves at a constant speed, the tether length is kept constant and the airplane is stationary when viewed in the carousel arm frame. As evident from Figure 2b, circular towing requires a lag of the airplane with respect to the towing arm. Due to the lag angle $-\phi$, the projection F_p of tether force vector F_c onto the carousel arm tip speed vector is non-zero. This allows work to be done by the carousel such that power is supplied to overcome drag of airplane and tether. More precisely, towing power transfer scales with $\frac{F_p}{F_c} = \sin(\phi)\cos(\theta)$.

As much as a non-zero ϕ is required to transmit power from the carousel to the tether, a non-zero ψ is needed to transmit power from the tether to the airplane. When drag

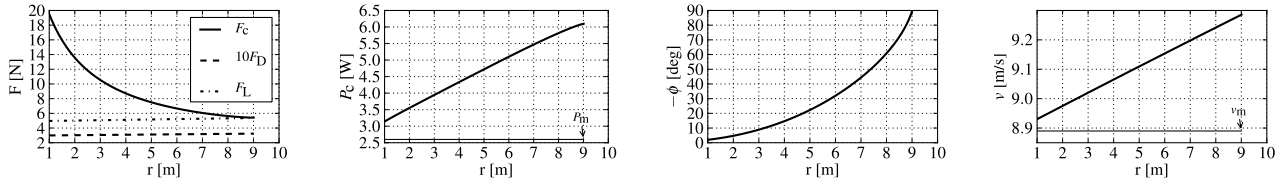

(a) Cable, Drag and Lift force (b) Carousel power (c) Lag angle (d) Effective wind speed

Fig. 3. Steady state results.

on the airplane rises, it will tend to seek regions of higher ψ.

The following set of equations applies to the case at hand:

$$\begin{cases} d^2 = L^2 + 2\cos(\phi) r L + r^2 & \text{cosine rule} \\ \sin(\psi) = -\sin(\phi) L/d & \text{sine rule} \\ F_\text{i} = mv^2/d & \text{inertia force} \\ F_\text{L} = AC_\text{L}\rho v^2/2 & \text{lift rule} \\ F_\text{D} = AC_\text{D}\rho v^2/2 & \text{drag rule} \\ \tan(\psi) = F_\text{D}/(F_\text{i} + F_\text{L}/\sqrt{2}) & \text{force balance} \end{cases}$$

The *force balance* equation simplifies to $\tan(\psi) = \frac{C_\text{D}}{C_\text{L}\sqrt{2}}$ for $r \to \infty$ i.e. ψ tends to a non-zero constant. Using the same limit, the *sine rule* tells us that the maximum ψ, attained for $\phi \approx -\frac{\pi}{2}$, amounts to $\psi \approx \frac{L}{r}$ i.e. a vanishingly small angle. The resulting contradiction proves that the circular towing scheme cannot be sustained in the limit of long tether. Equating the two limits results in a scale law that relates parameters for different systems that have identical ability to tow the airplane:

$$\frac{r}{L} \propto \frac{C_\text{L}}{C_\text{D}} \tag{1}$$

For an airplane in horizontal steady state free-flight, gravity gm is balanced by lift F_L. This balance dictates the nominal stall speed, v_m, and the minimal power required to keep the airplane airborne, P_m:

$$v_\text{m} = \sqrt{2gm/(\rho A C_\text{L})} \tag{2}$$

$$P_\text{m} = v_\text{m} F_\text{D} = \sqrt{2(gm)^3/(\rho A)}.C_\text{D}/C_\text{L}^{3/2} \tag{3}$$

Using the numbers from Table I, we obtain $v_\text{m} \approx 8.9\,\text{m/s}, P_\text{m} \approx 2.6\,\text{W}$. These numbers form a lower bound for results in the following section.

B. Circular towing numerical results

Let us formulate the problem of finding an efficient circular towing orbit as a non-linear optimization problem:

$\underset{\underline{q},\underline{u}}{\text{minimize}}$	P_c	minimize power supplied by carousel
subject to	$\theta = 0$	level flight
	$\dot{\delta}, \ddot{r}, \dot{C}_\text{L}, \dot{R} = 0$	zero input levels
	$\dot{\phi}, \dot{\theta}, \ddot{\phi}, \ddot{\theta} = 0$	stationarity of core states
	$\dot{r} = 0$	stationarity of tether length
	$-1.7 \leq \phi \leq 0$	limit lag angle
	$R \leq 0$	have the plane fly *the right way up*
	Constraints of Table III	
	Point model ODE	

Figure 3 shows the solution of this problem for increasing tether length r. Note how in Figure 3d the stall speed increases, since the lenghtening of the tether results in an increase in the mass of the system. Together with the increased drag, the required towing power increases quickly, as seen in Figure 3b. While equation (1) predicts a feasibility limit of the order of $r \approx 17\,\text{m}$. Detailed numerical analysis shows that no solutions exist after $r \approx 9\,\text{m}$, where ϕ tends to $\frac{\pi}{2}$ in Figure 3c.

C. Reversed pumping as a solution

The previous paragraphs indicate that an additional mechanism is needed to supply power to the airplane for large tether lengths. This power could come from 1) external wind if sufficiently strong near ground-level 2) an on-board propeller, requiring also batteries or a conducting tether 3) work done by the winch i.e. reversed pumping. This last option is what we consider in this paper.

Consider the simplified pumping scheme depicted in Figure 2c and 2d, in which with the airplane is switched between *relax* and *pull* modes with a duty cycle of 50%. The mean power that can be delivered to the kite is $(F_{c,\text{push}} - F_{c,\text{pull}})|\dot{r}|$. The force difference in this expression is equal to the change in lift vector. Mean power supply therefore scales with $\dot{r} C_\text{L} v^2$, while mean power loss is proportional $C_\text{D} v^2 v$. Equating these two proportions leads to

$$\frac{C_\text{L}}{C_\text{D}} \propto \frac{v}{\dot{r}} \tag{4}$$

Balancing of mean power is not a sufficient condition for feasibility of reversed pumping. During the relaxing phase, the system does work on the winch. Total mechanical energy at the start of the pulling must be enough to deliver this work and the work done by drag. The number of required cycles per revolution can be seen to scale with r.

V. Reversed pumping

This section suggests a problem formulation to find *reversed pumping* orbits. The found orbits are discussed and we report on the numerical methods and initialization strategy used to find them.

A. Numerical methods

All simulations and optimizations in this paper are performed with the `ACADO Toolkit`, developed by Boris Houska and Hans Joachim Ferreau [8]. This toolkit allows optimization problems to be written in a very natural way. The software reduces optimal control problems (OCP) to non-linear programs (NLP) via Bock's direct multiple shooting method [14] and solves them with an SQP method.

B. Problem formulation

For the *basic* scenario of reversed pumping, we formulate the following OCP:

$$\min_{\underline{\mathrm{q}}(t),\underline{\mathrm{u}}(t)} \underbrace{\frac{E_\mathrm{c}(T)}{T\dot{E}_\mathrm{c}^\star}}_{\text{mean power added by the carousel}} + \underbrace{\frac{E_\mathrm{w}(T)}{T\dot{E}_\mathrm{w}^\star}w_w}_{\text{mean power added by the winch (weighed)}} - \underbrace{\frac{E_\mathrm{p}(T)}{E_\mathrm{p}^\star}w_p}_{\text{potential energy of airplane (weighed)}}$$

s.t.	$[\phi,\theta,\dot{\phi},\dot{\theta},r,\dot{r},R,C_\mathrm{L}]^T(0)$ $= [\phi,\theta,\dot{\phi},\dot{\theta},r,\dot{r},R,C_\mathrm{L}]^T(T)$	periodicity of core & control states
	$8 \leq r[\mathrm{m}] \leq 20$	desired tether length of order 10 m
	$-0.5 \leq \phi[\mathrm{rad}] \leq 0.5$	limit lag
	$0 \leq \theta[\mathrm{rad}] \leq 1.5$	fly above carousel arm level
	$[E_\mathrm{c}, E_\mathrm{w}, \Xi_\mathrm{p}]^T(0) = 0$	energy integration from zero
	$E_\mathrm{c}(T) \geq 0$	avoid net energy transfer from winch
	$\delta(0) = 0$	phase invariance
	Constraints of Table III	
	Point model ODE	

This OCP tries to promote some desirable characteristics of reversed pumping orbits:

1) reaching higher values of r – we aim for the $10-20$ m range – than achievable by pure towing, promoted with a path constraint on r.
2) reaching a high altitude where wind would be stronger, promoted with the potential energy objective weight $w_p \approx 1$
3) using the winch as the dominant source of power, promoted by a relatively low weight on winch power $w_w \approx 1\times10^{-2}$.

The potential energy objective takes away remaining phase invariance: the solution is constrained to attain it's maximum height at $t = 0$ or $t = T$.

C. Initialization strategy

To solve a complex non-linear OCP, an initialization for states and controls is required. We start with the steady state circular towing NLP problem of Section IV-B for a tether length of $r = 1$ m. The radius is then iteratively increased and the according new equilibrium is computed, until the problem becomes infeasible.

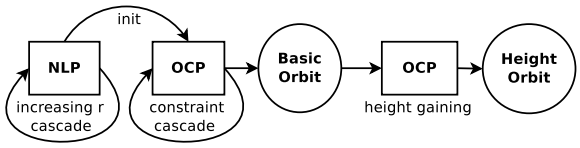

Fig. 5. State representation of the proposed cascade system. The basic orbit at $r \sim 10$ m is used to initialize a height-winning OCP.

The resulting circular orbit with the largest r was used to initialize the OCP. Imposing all of the constraints of Table III at once made the search for the optimum infeasible. The model was therefore equipped with several constraint sets of increasing strength. The solution of the OCP is fed recursively to `ACADO Toolkit`, each time adding or tightening constraints. The initial circular orbit is processed in this way by a cascade of models, resulting in the *basic* orbit which optimizes the basic OCP problem.

The *basic* cascade starts with a time-varying OCP, in which end time T is added to the decision variables. A longer cycle period allows for smaller velocities and accelerations, and for pumping cycles with greater variety in tether length. We chose the period of the cycle $\omega \times T$ to be π. In the rest of the chain, T is fixed to achieve faster convergence.

Next, we attempt to find a transient trajectory to launch the airplane. In a variant of the basic OCP, we replace the potential energy object by objectives for the tether length increase $r(T) - r(0)$ and inclination angle increase $\theta(T) - \theta(0)$. The periodicity constraints on these states are no longer required. A new periodic constraint on the kinetic energy is added to make the transient trajectory repeatable, yet sustainable: at the end of the transient, the airplane has the same capabilities to go through another transient. We refer to the resulting orbit as the *height gaining* orbit.

D. Discussion of the obtained results

The most important result is the existence of reversed pumping orbits that are feasible on our test setup. Figure 4 shows the obtained orbits for two scenarios. The time line is divided into quadrants, for $\delta + \phi = [0, \frac{\pi}{2}, \pi, \frac{3\pi}{2}]$. Figure 4g offers a visualisation of one orbit.

The basic orbit is a mode of operation with a fast descent, and a slow ascent. During the first and third quadrant, air speed is greatly increased, due to the simultaneous loss of altitude and retraction of the tether. It remains an open question why an objective that minimizes energy would favor this mode, because high speed induces high drag loss.

In the height gaining scenario, comparatively more energy is required. The winch uses an extra 10 J, and the carousel 3.35 J. The tether is lengthened by ~ 1 m, while inclination stays about the same. This results in a net gain of 3.38 J. Think of the potential energy as the output, and the winch and carousel energy as the input. We can then calculate their ratio as a measure of efficiency, which yields $\eta_E \approx 25\%$.

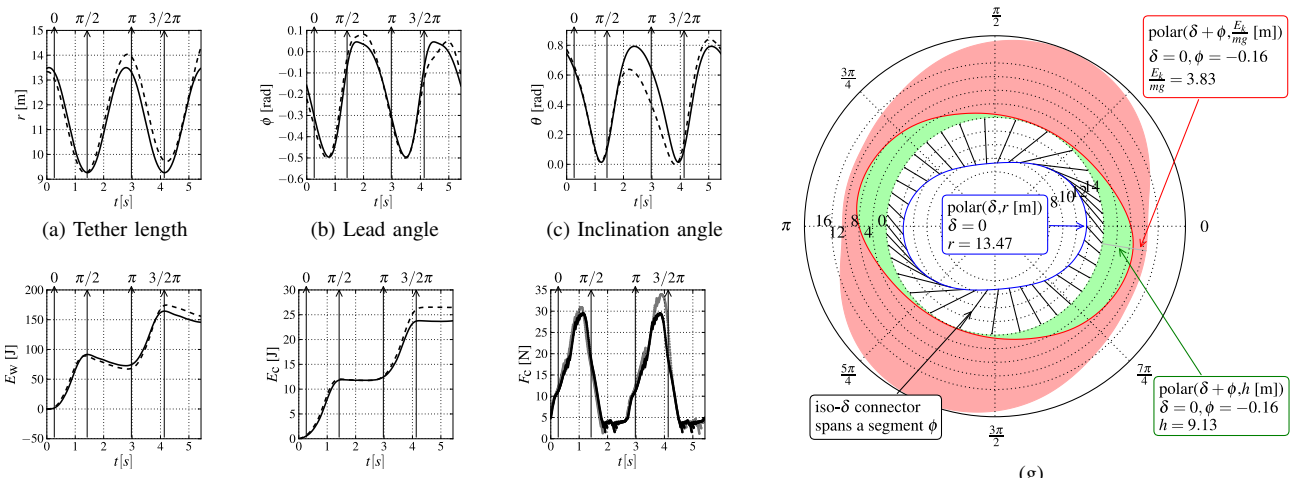

(a) Tether length (b) Lead angle (c) Inclination angle

(d) Energy of the winch (e) Energy of the carousel (f) Tether tension

(g)

Fig. 4. Reversed pumping trajectories. (a) through (e) time series of important system quantities. The full/black line denotes the *basic* orbit and the dashed/gray line outlines the *height gaining* orbit. The vertical grid lines denote the 4 key positions, where the airplane is immediately above an axis of the world frame, at $\delta + \phi = [0, \frac{\pi}{2}, \pi, \frac{3\pi}{2}]$. (f) Polar representation of *basic* orbit. Blue inner line shows tether length. The two colored bands depict mechanical energy as equivalent height. The width of the inner band denotes height, the width of outer band denotes kinetic energy. The blue inner line is plotted as a function of carousel angle δ. The bands are plotted as a function of the airplane angle $\delta + \phi$. The connector lines visualize the difference $-\phi$, i.e. the lag.

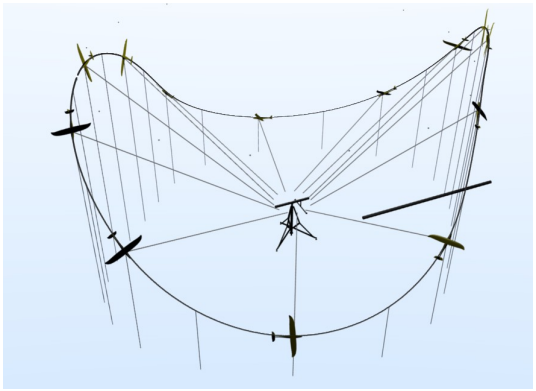

Fig. 6. Visualization of the *basic* trajectory. Horizontal bar indicates where $\delta = 0$. Airplane not to scale.

VI. Conclusion

We found that the previously proposed rotational start-up scheme, which uses circular towing, must be complemented with a reversed pumping strategy for larger tether lengths. We found both period and transient reversed pumping orbits by solving the proposed OCP that minimizes carousel supplied average power.

Acknowledgments

Supported by: RC-KUL: PFV/10/002 (OPTEC), IOF-SCORES4CHEM, GOA/10/9, GOA/10/1; FWO: G.0320.08, G.0558.08, G.0377.09; BelSPO IUAP P6/04 DYSCO; EU-FP7: HD-MPC, EMBOCON, ITN-SADCO, ERC-HIGHWIND; viCERP, ACCM.

References

[1] M. Diehl and B. Houska, "Windenergienutzung mit schnell fliegenden Flugdrachen: eine Herausforderung für die Optimierung und Regelung - Wind Power via Fast Flying Kites: a Challenge for Optimization and Control," *at-automatisierungstechnik*, vol. 57, no. 10, pp. 525–533, 2009. [Online]. Available: http://www.kuleuven.be/optec/files/Diehl2009d.pdf

[2] M. Loyd, "Crosswind Kite Power," *Journal of Energy*, vol. 4, no. 3, pp. 106–111, July 1980.

[3] "Plane Power Concept website," http://www.ampyxpower.com, 2012.

[4] M. Canale, L. Fagiano, M. Milanese, and M. Ippolito, "KiteGen project: control as key technology for a quantum leap in wind energy generators," in *Proceedings of the 2007 American Control Conference*, 2007. [Online]. Available: http://kitegen.com/

[5] Joby Energy, "Joby Energy Homepage." [Online]. Available: http://www.jobyenergy.com/

[6] I. Argatov and R. Silvennoinen, "Energy conversion efficiency of the pumping kite wind generator," *Renewable Energy*, vol. 35, pp. 2052 – 1060, 2010.

[7] P. Williams, B. Lansdorp, and W. Ockels, "Optimal Crosswind Towing and Power Generation with Tethered Kites," *Journal of Guidance, Control, and Dynamics*, vol. 31, no. 1, pp. 81–92, January–February 2008.

[8] B. Houska, H. Ferreau, and M. Diehl, "ACADO Toolkit – An Open Source Framework for Automatic Control and Dynamic Optimization," *Optimal Control Applications and Methods*, 2011, dOI: 10.1002/oca.939 (in print).

[9] SkySails, "SkySails Homepage," http://www.skysails.info. [Online]. Available: http://www.skysails.info

[10] K. Geebelen and J. Gillis, "Modelling and control of rotational start-up phase of tethered aeroplanes for wind energy harvesting," Master's thesis, K.U.Leuven, June 2010. [Online]. Available: http://www.kuleuven.be/optec/files/Geebelen2010.pdf

[11] M. Diehl, "Real-Time Optimization for Large Scale Nonlinear Processes," Ph.D. dissertation, Universität Heidelberg, 2001, http://www.ub.uni-heidelberg.de/archiv/1659/.

[12] B. Houska, "Robustness and Stability Optimization of Open-Loop Controlled Power Generating Kites," Master's thesis, University of Heidelberg, 2007. [Online]. Available: http://www.kuleuven.be/optec/files/Houska2007a.pdf

[13] R. Lozano *et al.*, "Demonstration of small-scale indoor reversed pumping," 2011, unscheduled presentation at AWEC 2011 conference.

[14] H. Bock and K. Plitt, "A multiple shooting algorithm for direct solution of optimal control problems," in *Proceedings 9th IFAC World Congress Budapest*. Pergamon Press, 1984, pp. 243–247. [Online]. Available: http://www.iwr.uni-heidelberg.de/groups/agbock/FILES/Bock1984.pdf